High-throughput measurement of rice tillers using a conveyor equipped with x-ray computed tomography

Wanneng Yang, Xiaochun Xu, Lingfeng Duan, Qingming Luo, Shangbin Chen, Shaoqun Zeng, and Qian Liu[a)]
Britton Chance Center for Biomedical Photonics, Wuhan National Laboratory for Optoelectronics-Huazhong University of Science and Technology, Wuhan 430074, China

(Received 31 August 2010; accepted 6 December 2010; published online 7 February 2011)

Tillering is one of the most important agronomic traits because the number of shoots per plant determines panicle number, a key component of grain yield. The conventional method of counting tillers is still manual. Under the condition of mass measurement, the accuracy and efficiency could be gradually degraded along with fatigue of experienced staff. Thus, manual measurement, including counting and recording, is not only time consuming but also lack objectivity. To automate this process, we developed a high-throughput facility, dubbed high-throughput system for measuring automatically rice tillers (H-SMART), for measuring rice tillers based on a conventional x-ray computed tomography (CT) system and industrial conveyor. Each pot-grown rice plant was delivered into the CT system for scanning via the conveyor equipment. A filtered back-projection algorithm was used to reconstruct the transverse section image of the rice culms. The number of tillers was then automatically extracted by image segmentation. To evaluate the accuracy of this system, three batches of rice at different growth stages (tillering, heading, or filling) were tested, yielding absolute mean absolute errors of 0.22, 0.36, and 0.36, respectively. Subsequently, the complete machine was used under industry conditions to estimate its efficiency, which was 4320 pots per continuous 24 h workday. Thus, the H-SMART could determine the number of tillers of pot-grown rice plants, providing three advantages over the manual tillering method: absence of human disturbance, automation, and high throughput. This facility expands the application of agricultural photonics in plant phenomics. © *2011 American Institute of Physics*. [doi:10.1063/1.3531980]

I. INTRODUCTION

Rice is a primary food source whose yield is determined by the number of tillers and panicles per plant, the number of grains per panicle and grain weight.[1] Generally, tillering is one of the most important agronomic traits because the number of shoots per plant determines panicle number, a key component of grain yield.[2] Rice tillers, including primary, secondary, and tertiary tillers, are produced by the outgrowth of axillary buds to form shoot branches. From an agronomic perspective, grain yield is usually dictated by the primary tillers as well as some early secondary tillers, whereas tertiary and late secondary tillers make little contribution despite consuming nutrients, water, and photosynthates.[3]

In rice breeding, it is imperative that the phenotype of the tillers, resulting from gene hybridization or mutation, is monitored and analyzed. Modern crop breeding methods using genetically modified organisms are able to produce hundreds of new varieties daily, so efficient techniques for screening candidate plant materials are critical.[4] The Plant Accelerator at the University of Adelaide (Adelaide, Australia), in operation since January 2010, is designed for a throughput of 2400 plants per day. Meanwhile, the plant phenomics facility, called Smarthouse, consists of greenhouses coupled with imaging facilities, including infrared, visible light, and fluorescence imaging.[5] Using these high-throughput phenotyping techniques, some plant traits can be extracted, such as leaf area, leaf temperature, and plant height, but not tiller number.[6] The conventional method for counting tillers is still manual, which is not only time consuming but also subjective. Since the intact tillers of rice plants usually overlap, visible light imaging cannot detect some of the inner tillers, even though pot-grown rice plants are rotary for multiangle imaging. Therefore, a means of automatic, noncontact measurement of tiller number is desirable.

X-ray computed tomography (CT) is a modern slice-imaging modality widely used in medicine, industrial practice, and molecular imaging.[7–11] We designed a novel system based on x-ray CT to count the tillers of pot-grown rice plants, termed the high-throughput system for measuring automatically rice tillers (H-SMART). Previously, our group also applied micro-CT technology to measure the number of tillers on rice plants,[12] proving the feasibility of using CT to achieve this purpose. However, the micro-CT system is too expensive for commercialization and could only be regarded as a prototype. Therefore, in this study, we expanded our system's utility by investigating x-ray CT as an alternative to micro-CT, which provides higher throughput, higher measurement accuracy, and lower cost.

a)Author to whom correspondence should be addressed. Electronic mail: qianliu@mail.hust.edu.cn. Tel: +86 27 87792033. Fax: +86 27 87792034.

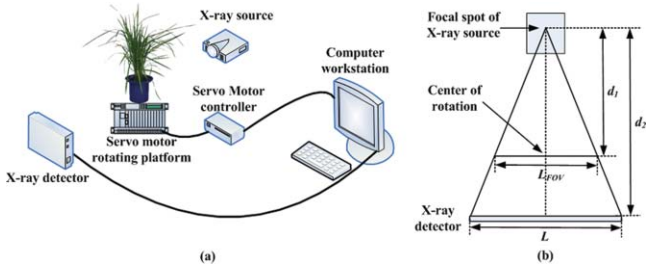

FIG. 1. (Color online) Schematic (a) and configuration (b) drawings of the x-ray CT system for the measurement of rice tillers. The fan-beam x-ray source and line-array x-ray detector were used to obtain the transverse section image of culms of rice planted in a pot.

II. SYSTEM DESCRIPTION

A. X-ray CT system

The H-SMART system is based on industrial CT. Figure 1(a) shows a schematic drawing of the x-ray CT system, consisting of an x-ray source, an x-ray detector, a rotating platform, a servo motor controller, and a computer workstation. The specimen (i.e., pot-grown rice plant) is placed on the rotating platform driven by the servo motor, while the x-ray source and detector remain stationary. The computer workstation (HP xw6400, Hewlett-Packard Development Company, USA) regulates the servo motor controller (MBDDT2210, Panasonic Corporation, China), driving the uniform spin of the rotating platform continuously. For practical reasons, a commercial fan-beam x-ray source and linear-array x-ray detector are used (T80-1-60 and x scan 0.4f3-205, respectively, both from BMEI Co. Ltd, China). The x-ray source holds a focal spot size of about 0.8 mm with an affixed tungsten anode, and the operation voltage and current range of the source are 40–80 kV and 0.2–1 mA, respectively. Details pertaining to the linear-array detector used here are shown in Table I.

The system geometry and characteristics are exhibited in Fig. 1(b). The distance d_1 between the x-ray focal spot and center of rotation is 1122 mm. The distance d_2 between the x-ray focal spot and detector is 1412 mm. The length of detector (768 detector elements) L is 307 mm. Hence, the magnification factor M is approximately 1.26, calculated by d_2/d_1, and the transaxial field of view (FOV) L_{FOV} is 244 mm, calculated by L/M.

TABLE I. Main characteristics of the linear-array x-ray detector.

Characteristic	X scan 0.4f3-205
X-ray tube voltage range (kV)	20–160
Scintillator material	GOS (Gadolinium oxysulfide)
Number of pixels	768
Pixel pitch (mm)	0.4
Pixel height (mm)	0.6
Pixel width (mm)	0.3
Maximum scanning speed (cm/s)	80
A/D resolution (bit)	14
Saturation signal/RMS noise	>2000

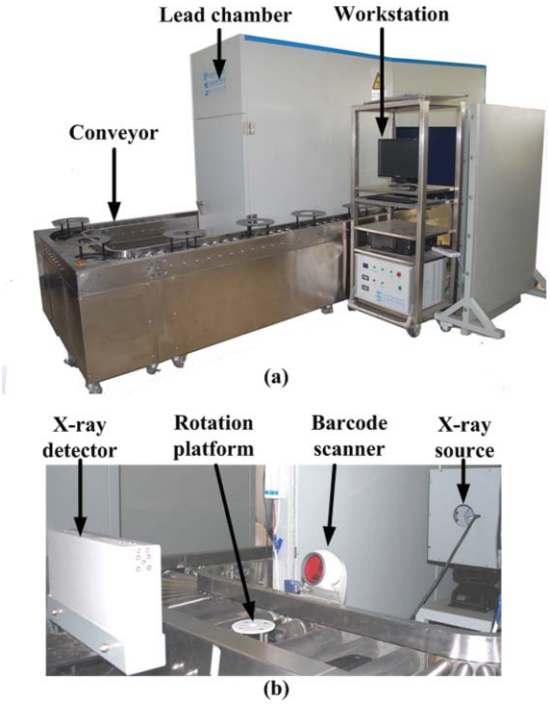

FIG. 2. (Color online) Real images of the entire H-SMART (a) and x-ray CT system (b) The x-ray CT system is the core part of the H-SMART, which is fixed in a lead chamber.

B. High-throughput facility

To achieve high throughput, a single industrial conveyor [Fig. 2(a)] is used to deliver pot-grown rice plants to the x-ray CT system [Fig. 2(b)] automatically. For safety, a lead chamber is constructed for x-ray radiation shielding, and the CT system is fixed in the chamber [Fig. 2(a)]. In a practical working environment, where the voltage and current range of the x-ray source are 50 kV and 1 mA, respectively, the maximum dose equivalent rate of the work area is 0.06 μSv/h, as tested by the Hubei Institute of Measurement and Testing Technology. The transportation lineout of the chamber provides an interface for inputting the rice plant pots for CT scanning. Meanwhile, the conveyor not only enables measurement but also separates the rice input area from the CT scanning area for improved radiation safety. A barcode on each pot, read with a barcode scanner [MS7120, Honeywell International Incorporation, shown in Fig. 2(b)], is used for indexing tiller measurement results, which are then stored as a Microsoft Excel file.

C. System control

The computer workstation, with software developed in LABVIEW 8.6 (National Instruments, USA), is operated for whole system control, including transportation control, image acquisition and processing, and results display and storage. The control flowchart is illustrated in Fig. 3, which includes the following steps: (1) the new pot-grown rice is transported to the rotation platform; (2) the rotation platform rises to a preset point; (3) the x-ray system collects images as the pot-grown rice rotates continuously; (4) after acquisition, the

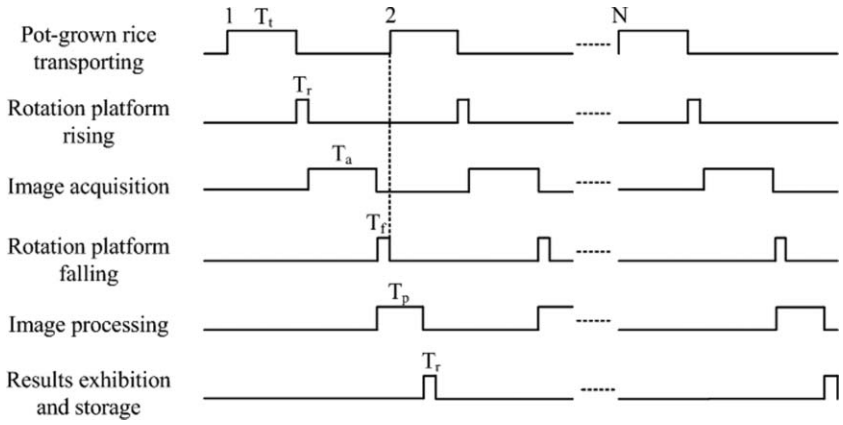

FIG. 3. Control flowchart of the H-SMART.

images are processed to determine the number of tillers and the rotation platform returns to its original position; and (5) the recently examined rice is transported away from the system and the next pot arrives on the rotation platform.

The time consumption of rice transport, image acquisition, and rotation platform rising and falling (denoted by T_t, T_a, T_r, and T_f, respectively) is designed to be 9, 9, 1, and 1 s, respectively. Additionally, it takes about 5 s to complete the entire image processing computation with the computer workstation configured with 2.3 GHz main frequency, 3 GB memory, and four CPU processors. Beside the image computation, the computer workstation performs results exhibition and storage, which requires less than 1 s. Therefore, the approximate tiller-number extraction time per rice plant (T) is 20 s, calculated using the following equation:

$$T = T_t + T_r + T_a + T_f. \tag{1}$$

The H-SMART operates in a quasicontinuous manner, with its work flow including pot-grown rice plant input, CT

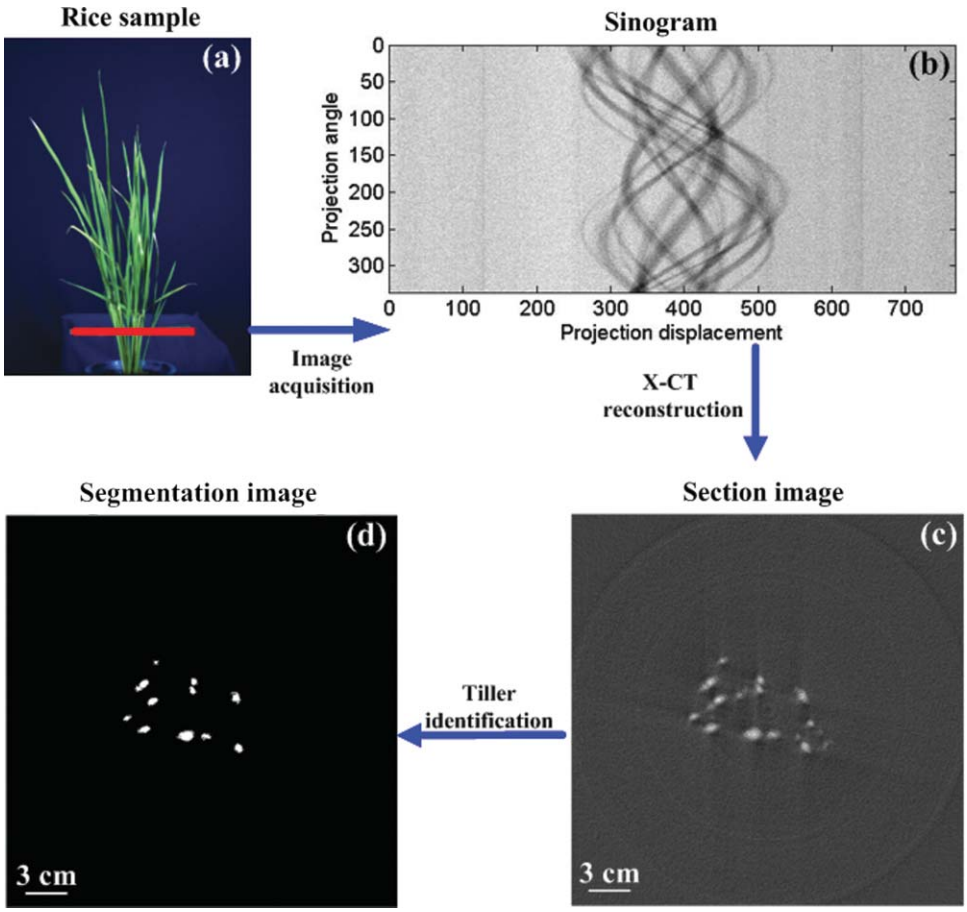

FIG. 4. (Color online) Procedural framework of image processing in the present system. The filtered back-projection algorithm was used to reconstruct the sinogram (b) into the section image (c). The segmentation method was then used to identify the number of tillers (d).

scanning, determination of the tiller number, and pot-grown rice plant output.

III. IMAGE PROCESSING

The rice plant culms are scanned by the fan-beam x ray. One-dimensional projection data for the part of the culms approximately 50 mm above the pot height, where most primary tillers and some early secondary tillers are located, are obtained at each projection angle [Fig. 4(a)]. During the period of platform rotation, the computer acquires the entire sinogram, covering 336 orientations (step angle 0.85°, entire angle 0.85°×336, ~285.60°), for about 9 s. The size of the sinogram is 336 × 736 pixels [Fig. 4(b)].

The conventional filtered back-projection (FBP) algorithm is applied to reconstruct the transverse section image of the rice culms [Fig. 4(c)]. More specifically, in the case of fan-beam reconstruction, the FBP algorithm comprises two stages: preweighted convolution filtering and weighted back projection.[13–18] Basic image processing methods, such as a median filter for image denoising, a threshold operator for image segmentation, and several morphological operators (filling hole, erosion, watershed, etc.), are then applied to identify the tillers in the section image [Fig. 4(c)]. The number of tillers of the target rice plant could be obtained automatically from the resultant image [Fig. 4(d)]. The detailed processes of both CT reconstruction and tiller identification, respectively, are described below.

A. CT reconstruction algorithm

Here, the FBP algorithm is used for image reconstruction. Under the conditions of equidistant detector elements and a fan-beam x ray, the FBP algorithm[8] comprises two steps. The first is preweighted convolution filtering, described by the equation

$$\tilde{P}(\beta, a) = \left(P(\beta, a) \frac{R}{\sqrt{R + a^2}} \right) * h(a), \tag{2}$$

where β is the projection angle; a is the projection displacement on the virtual plane $D'_1D'_2$, corresponding to the real plane of detector D_1D_2, as shown in Fig. 5; $p(\beta,a)$ indicates the original projection data; R is the distance between the x-ray spot S and rotation center O; and to maintain resolution, a Ram–Lak filter (also known as a ramp filter) is also included as the convolution filter $h(a)$.[9]

For the second step, to reconstruct voxel $f(x, y)$, the process of weighted back projection is described as

$$f(x, y) = \int_0^{2\pi} \frac{R^2}{U(x, y, \beta)^2} \tilde{P}[\beta, a(x, y, \beta)] d\beta, \tag{3}$$

where a and U (indicated in Fig. 5) are computed as

$$a(x, y, \beta) = R \frac{-x \sin\beta + y \cos\beta}{R + x \cos\beta + y \sin\beta}, \tag{4}$$

$$U(x, y, \beta) = R + x \cos\beta + y \sin\beta. \tag{5}$$

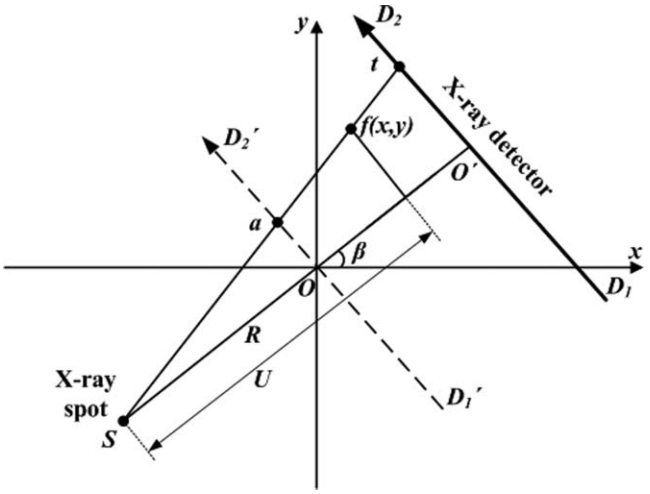

FIG. 5. Geometric diagram of the CT reconstruction algorithm.

Moreover, for the purpose of noise reduction, the projection data (also known as a sinogram) is normalized before image reconstruction using the equation

$$I_N = \log \frac{I - I_D}{I_0 - I_D}, \tag{6}$$

where I is original projection data acquired from the linear x-ray detector; I_0 and I_D are the blank and dark current projections, respectively, used for normalization purposes; and I_N is the normalized projection data.[19]

B. Tiller identification

The flow chart of image processing for identification of rice tillers is outlined in Fig. 6. Due to the presence of noise in the original reconstructed image, stemming from the

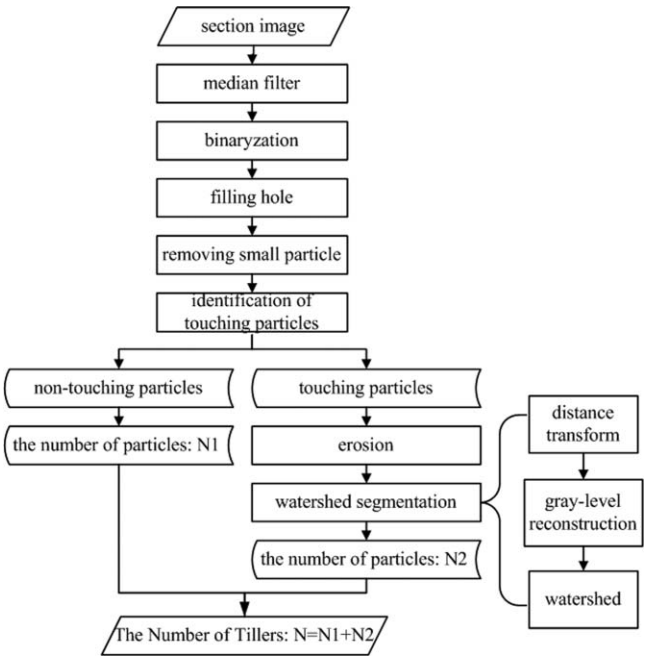

FIG. 6. Flowchart of tiller identification.

sinogram, a median filter is used to denoise. Then, to divide the gray image into the background and foreground, it is segmented into a binary image, using a fixed threshold. Through preliminary experiments, an appropriate gray value was selected as the threshold. Due to the presence of hollow medullary cavities in the rice stems, some objects in the binary image may appear holey. Hence, the filling-holes operation helps to maintain a consistent size and shape for all objects. Next, too small objects that are not tillers must be removed.

After this image processing, we identify the touching objects according to the length-width ratio of each individual object. The number of nontouching objects is denoted by N_1. erosion and watershed segmentation is used to separate the touching objects, improving the accuracy of counting the touching tillers. To minimize the oversegmentation effect, the process of watershed segmentation includes three parts: distance transform, gray-level reconstruction, and watershed. The resultant number of separated touching objects is denoted as N_2. Finally, the number of tillers is calculated based on the equation N_1+N_2.

IV. RESULTS

Three batches of rice at different growth stages (tillering, heading, or filling) were used to test the precision of the H-SMART. Each batch contained 50 pots of rice plants belonging to the japonica variety Zhonghua 11.

Variety identification (mutant versus wild) is one of the interesting features of the H-SMART. To confirm this application, 2830 pots of rice plants at the filling stage,

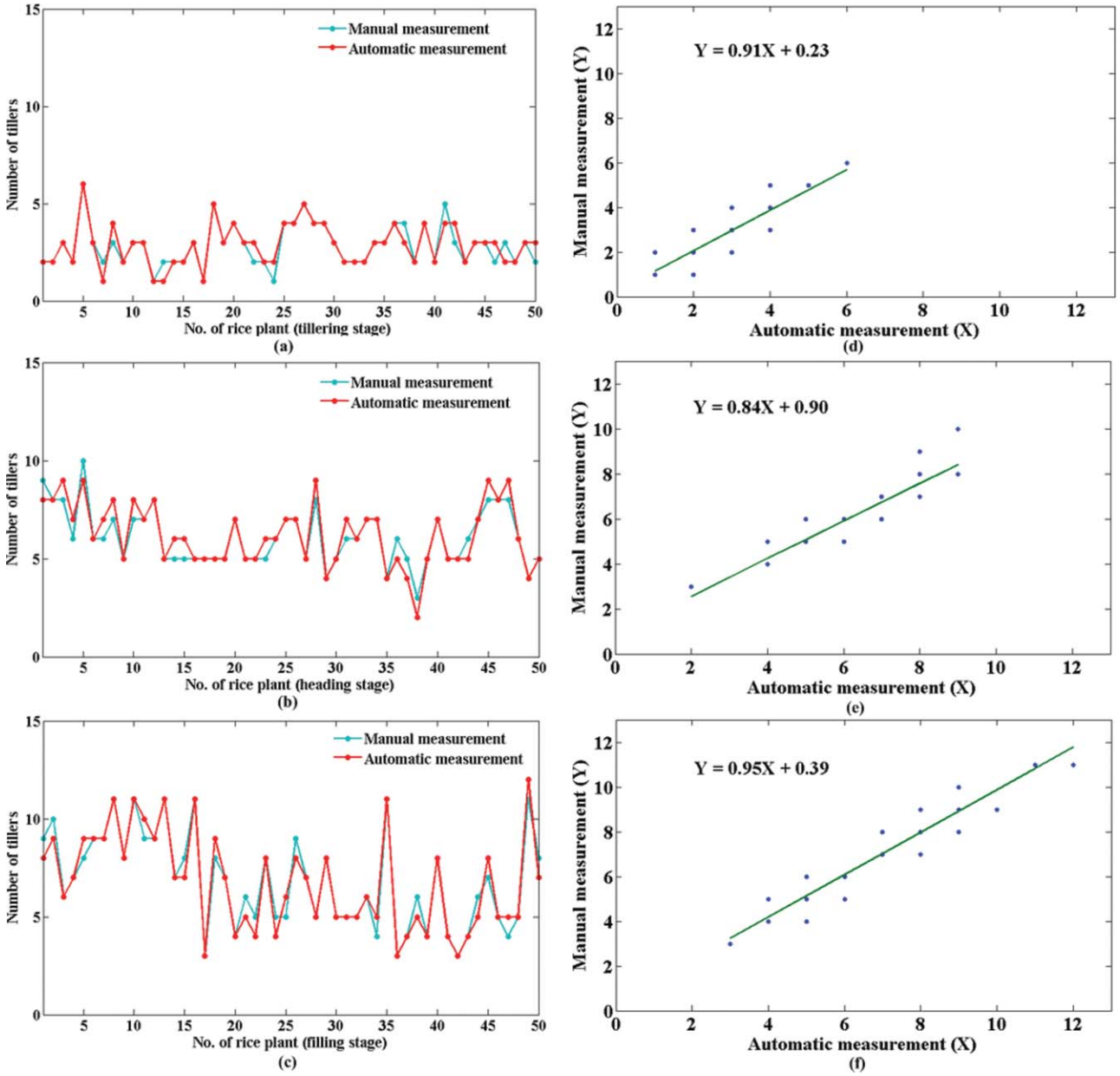

FIG. 7. (Color online) Results of manual measurement (pale color) vs automatic measurement (deep color) at three different stages: (a) tillering, (b) heading, and (c) filling. The scatter plots of measurement results at three different stages: (d) tillering, (e) heading, and (f) filling.

TABLE II. Regression analysis for automated observations (X) vs manual observations (Y).

Growth stage	Sample number	Regression equation	Related coefficient	Specified value (X_0)	Predicted value (Y_0)	95% Confidence interval for Y_0	
						Lower bound	Upper bound
Tillering stage	50	$Y = 0.91X + 0.23$	0.91	3	2.97	2.02	3.92
Heading stage	50	$Y = 0.84X + 0.90$	0.93	6	5.91	4.82	7.00
Filling stage	50	$Y = 0.95X + 0.39$	0.97	7	7.03	5.82	8.24
Filling stage under industry conditions	2830	$Y = 1.03X - 0.80$	0.98	11	10.56	6.19	14.94

which included mutant and wild plants, were used to test the H-SMART.

A. Measurement accuracy

To test the precision of the H-SMART, three batches of rice at different growth stages (tillering, heading, or filling) were automatically measured using this system. Most primary tillers and some early secondary tillers have at least two leaves;[3] therefore, merely tillers with two or more leaves were counted in manual measurement. Moreover, in order to identify the tillers as many as possible, after plenty of experiments, a proper segmentation threshold had been chosen for the image processing of binaryzation.

In the left half part of Fig. 7, the results of manual counting (cyan lines) by experienced staff are displayed together with the automatically acquired results (red lines), indicating that the absolute error for each rice plant sample is within ±1.

The mean absolute error [MAE, defined below by Eq. (7)] of the manual and automatic measurements at three different growth stages (tillering, heading, and filling) is 0.22, 0.36, and 0.36, respectively. And the root mean squared error [RMSE, defined below by Eq. (8)] at the three different growth stages are 0.47, 0.6, and 0.6, respectively,

$$\mathrm{MAE} = \frac{1}{n}\sum_{i}^{n} |x_{ai} - x_{mi}|, \tag{7}$$

$$\mathrm{RMSE} = \sqrt{\frac{1}{n}\sum_{i=1}^{n} (x_{ai} - x_{mi})^2}, \tag{8}$$

where x_{mi} is the manually measured value, x_{ai} is automatically measured value, and n is the number of plant samples.

In addition to supplement the statistical information on precision and accuracy, three scatter plots of different growth stages are illustrated in right half part of Fig. 7, respectively.

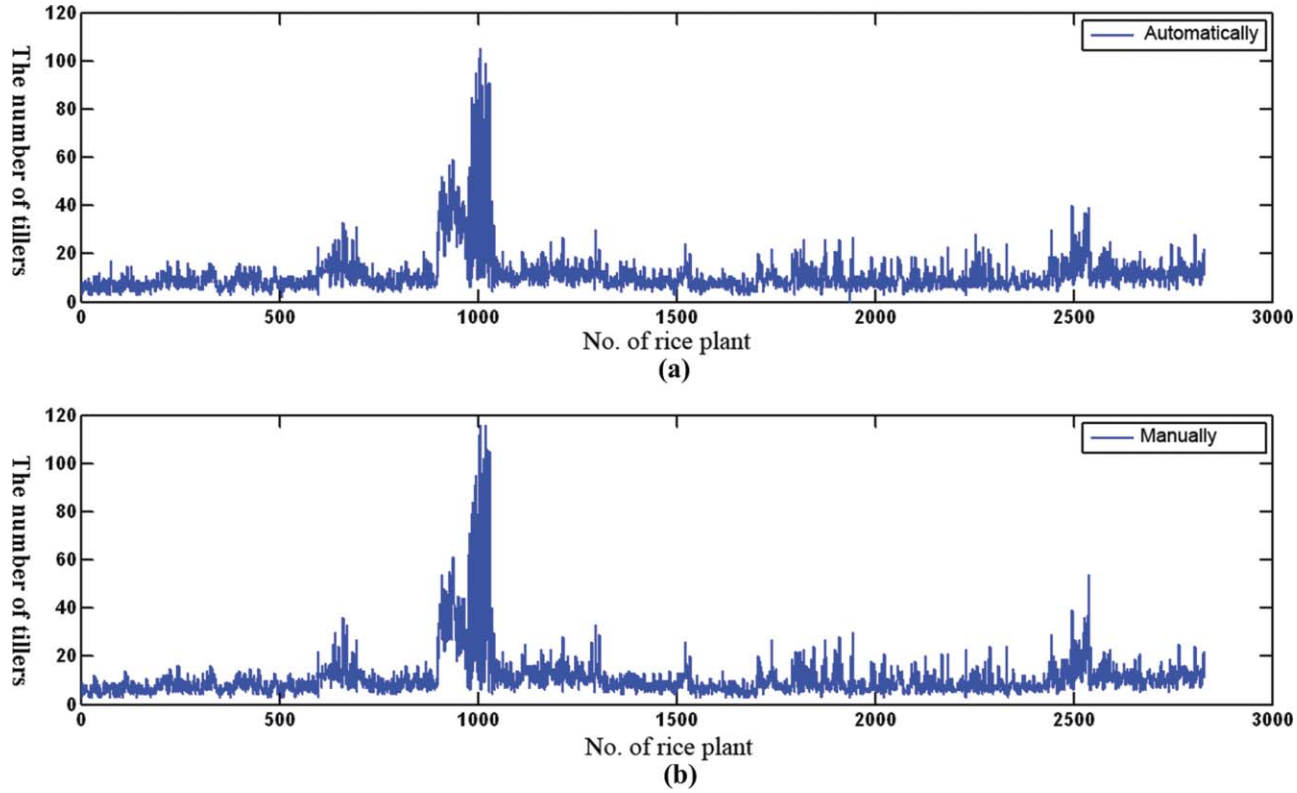

FIG. 8. (Color online) Number of rice tillers measured automatically (a) and manually (b). The rice plants with pot tags from 801 to 1050 were mutant, according to the number of tillers.

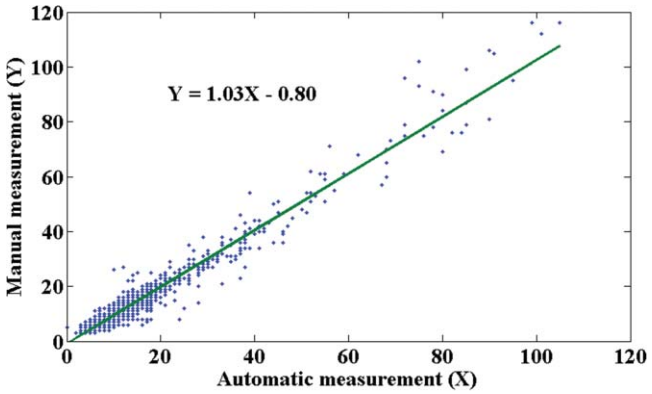

FIG. 9. (Color online) Scatter plot for automatic (X) vs manual (Y) observations of 2830 pots under industry conditions.

And the main results of complete regression analysis for automated observations (X) versus manual observations (Y) are shown in Table II. Given a specified value (mean value, X_0) and 95% confidence interval, the predicted value (Y_0) and predicted intervals could be calculated.

B. Measurement efficiency

To estimate the efficiency of the H-SMART for practical applications, 2830 pots of rice plants were tested both automatically and manually. The H-SMART required about 20 s per rice plant to perform a noncontact measurement and completed the measurements within 2 days, working 8 h per day. In comparison, the manual measurement required 2 days of counting by 10 personnel and involved hand-touch contact. The results of both measurements are shown in Fig. 8. The data are very similar, with a correlation coefficient of 0.98, indicating that the results of automatic measurement are essentially the same as those of manual measurement. Similarly, the liner regression analysis is applied for the obtained data of 2830 pots. The main results of regression analysis are shown in Table II, and the scatter plot is exhibited in Fig. 9. Thus, under the condition of 95% confidence interval, the regressive effect of automated observations (X) versus manual observations (Y) was significant as shown in the table.

The findings also demonstrate that the rice plants with tags numbered between 801 and 1050 were mutant varieties. Using the H-SMART, it is thus relatively easy to identify mutants according to significant differences in the number of rice tillers between the mutant and wild plants. Additionally, when continuously running all day, the mean time between failures (MTBF) of the H-SMART is 5 days and its throughput is designed for 4320 rice plants per continuous workday.

V. CONCLUSION AND DISCUSSION

Here, we demonstrate the use of a combination of x-ray CT and conveyor equipment to facilitate tiller counting. Equipped with specific software for system control and digital image processing, the H-SMART is able to determine the number of tillers of pot-grown rice plants, providing three major advantages over manual counting: absence of human disturbance, automation, and high throughput. The H-SMART system can be applied during rice breeding to screen mutants, in which it is ten times more efficient than human screening, enabling detection of a single relevant mutant among thousands of candidate rice plants. Additionally, if the resolution of the x-ray detector is sufficiently high, the morphological properties of individual tillers can also be extracted and analyzed from the reconstructed image. In the future, visible light imaging will be incorporated into the H-SMART to allow measurement of rice height, green leaf area, and tiller number. This system complies with the trend of plant phenomics, which strives to maximize breeding by applying imaging techniques from medicine to agriculture.[20] In sum, the H-SMART uses agricultural photonics to provide a novel tool for studying phenomics.

ACKNOWLEDGMENTS

The authors deeply appreciate the help of our collaborators at Huazhong Agricultural University with obtaining the rice plant samples. This work was supported by the National High Technology Research and Development Program of China (863 Program, Grant No. 2010AA10Z203), the Key Program of the Natural Science Foundation of Hubei Province (Grant No. 2008CDA087), and the Program for New Century Excellent Talents in University (Grant No. NCET-10-0386).

[1] W. Xue, Y. Xing, X. Weng, Y. Zhao, W. Tang, L. Wang, H. Zhou, S. Yu, C. Xu, X. Li, and Q. Zhang, Nat. Genet. **40**, 761 (2008).
[2] X. Li, Q. Qian, Z. Fu, Y. Wang, G. Xiong, D. Zeng, X. Wang, X. Liu, S. Teng, F. Hiroshi, M. Yuan, D. Luo, B. Han, and J. Li, Nature (London) **422**, 618 (2003).
[3] Y. Xing and Q. Zhang, Annu. Rev. Plant Biol. **61**, 421 (2010).
[4] M. Bagge and T. Lubberstedt, Mol. Breeding **22**, 319 (2008).
[5] H. Malte and L. Hauke, *Proceedings of the 20th International Conference on Automated Planning and Scheduling*, Toronto, Canada, 12–16 May 2010, (AAAI press, Menlo Park, California), p. 234.
[6] B. Bettina, P. Boris, and T. Mark, J. Exp. Bot. **61**, 3519 (2010).
[7] W. A. Kalender, Phys. Med. Biol. **51**, R29 (2006).
[8] A. C. Kak, and M. Slaney, *Principles of Computerized Tomographic Imaging* (IEEE, New York, 1988), pp.75–93.
[9] X. Yang, H. Gong, G. Quan, Y. Deng, and Q. Luo, Rev. Sci. Instrum. **81**, 054304 (2010).
[10] E. Krestel, *Imaging Systems for Medical Diagnostics* (Publicis Corporate Publishing, Erlangen, 2005), pp. 413–434
[11] F. Natterer, *The Mathematics of Computerized Tomography* (Wiley, New York, 1986), pp.102–119.
[12] Z. Fang, K. Bi, S. Zeng, Q. Luo, and Q. Liu, *Proceedings of the 6th International Conference on Photonics and Imaging in Biology and Medicine*, Wuhan, P. R. China, 4–6 November 2007, (World Scientific Publishing Company, Singapore), p. 237.
[13] D. L. Parker, Med. Phys. **9**, 254 (1982).
[14] G. T. Herman, Real-Time Imag. **1**, 3 (1995).
[15] D. Per-Erik and I. Malin, IEEE Nuclear Science Symposium **2**,1279 (1997).
[16] S. Basu and Y. Bresler, IEEE Transactions on Image Processing. **9**, 1760 (2000).
[17] J. Fu, H. Lu, and Q. Zhang, CT Theory Appl. **11**, 16 (2002).
[18] F. Noo, M. Defrise, R. Clackdoyle, and H. Kudo, Phys. Med. Biol. **47**, 2525 (2002).
[19] T. Benson and J. Gregor, *Proceedings of the IEEE Nuclear Science Symposium Conference Record*, Rome, Italy, October 2004, (IEEE press, California), p. 3253.
[20] E. Finkel, Science **325**, 380 (2009).